New Results

40 Hz acoustic stimulation decreases amyloid beta and modulates brain rhythms in a mouse model of Alzheimer's disease

Juho Lee[1,*], Seungjun Ryu[1,*], Hyun-Ju Kim[2], Jieun Jung[1], Boreom Lee[1,#], Tae Kim[1,3,#]

[1]Department of Biomedical Science and Engineering, Gwangju Institute of Science and Technology (GIST), Gwangju, South Korea; [2]Department of Brain Science, University of Ulsan College of Medicine, Seoul, South Korea; [3]School of Life Sciences, GIST, South Korea

[*]J.L. and S.R. contributed equally to this work. T.K. and B.L. contributed equally to this work.

[#]Correspondence should be addressed to T. K. or B. L. E-mail:

tae-kim@gist.ac.kr (T. K.), leebr@gist.ac.kr (B. L.).

Abstract

Introduction

The accumulation of amyloid-beta (Aβ) is one of the neuropathologic hallmarks of Alzheimer's disease (AD) and abnormal gamma band oscillations and brain connectivity have been observed. Recently, a therapeutic potential of gamma entrainment of the brain was reported by Iaccarino *et al.* However, the affected areas were limited to hippocampus and visual cortex. Therefore, we sought to test the effects of acoustic stimulation in a mouse model of AD.

Methods

Freely moving 6-month-old 5XFAD mice with electroencephalogram (EEG) electrodes were treated with daily two-hour acoustic stimulation at 40Hz for 2 weeks. Aβ and microglia were evaluated by immunohistochemistry and ELISA. Evoked and spontaneous gamma power were analyzed by wavelet analysis. Coherence, phase locking value (PLV), and cross-frequency coupling were analyzed.

Results

The number of Aβ plaques decreased in the pre- and infra- limbic (PIL) and hippocampus regions and soluble Aβ-40 and Aβ-42 peptides in PIL in the acoustic stimulation group. We also found that the number of microglia increased in PIL and hippocampus. In EEG analysis, evoked gamma power was decreased and spontaneous gamma power was increased. Gamma coherence and phase locking value did not show significant changes. Cross-frequency coupling was shifted from gamma-delta to gamma-theta rhythm.

Conclusion

In summary, we found that acoustic stimulation at 40Hz can reduce Aβ in the brain and restore the gamma band oscillations and the fronto-parietal connectivity. Our data suggest

47 that acoustic stimulation might alter the natural deterioration processes of AD and have a
48 therapeutic potential in AD.

49 Key Words: Gamma band oscillations, acoustic stimulation, amyloid beta, microglia, brain
50 connectivity, 5XFAD

Introduction

Alzheimer's disease (AD) is the most common cause of dementia [1-3] and understood as a complex disease that affects behavior and cognition through various pathophysiological mechanisms [4]. The deposition of amyloid-beta (Aβ) peptide is one of the major pathological findings associated with AD [5]. In AD, the balance between formation and clearance of Aβ is impaired [6]. Under normal physiological conditions, glia cells, especially microglia and astrocytes, play crucial roles in maintaining the balance. The aggregated Aβ is degraded by microglia and astrocyte [7] and the soluble Aβ is eliminated through the perivascular pathway [8-11]. In spite of recent failures of drug development targeting Aβ and skepticism, the 'amyloid hypothesis' are still one of the leading theory of AD pathogenesis [12].

Neuronal activity with gamma band (30-70 Hz) oscillations (GBO) in the human electroencephalogram (EEG) is known to be associated with human sensation, perception, cognitive process, such as information storage, retrieval, and integration [13-16]. Cortical GBO are produced by the interplay between inhibitory interneurons and excitatory pyramidal neurons cellular [17]. It is noteworthy that the patients with AD have shown abnormal GBO. Several studies have reported decreased activity of the spontaneous GBO in AD [18,19]. The synchronization in spontaneous GBO was also suppressed compared to healthy controls [19,20]. In contrast, evoked GBO as a steady-state response (SSR) to the repeated visual, auditory or somatosensory stimuli at a certain frequency increased in patients with AD [21-23].

The deposition of Aβ impairs synaptic plasticity at glutamatergic synapses, forms a synaptic depression with the morphological change of dendritic spine [24,25], and the GBO [26]. Therefore, immunotherapy has been conducted aiming at the reduction of accumulated Aβ. Intracranial or systemic administration of immunotherapeutic agents reduced Aβ deposition by mechanisms both associated with and independent of microglial activation [27,28]. Following

studies have reported decreased Aβ plaques, increased soluble Aβ and altered shape of dystrophic neurite [29-33]. However, immunotherapy did not improve the overall survival in phase 1 clinical trials with side effects [34].

The functional abnormalities of PV neuron and fast-spiking basket cells are origins of abnormal function of GBO [35]. In mice with the mutated APP, damaged PV cells produce network dysfunction. Restoration of the interneuron-specific and PV cell predominant voltage-gated sodium channel (VGSC) subunit improved recovery of gamma oscillation and memory impairment and also resulted in improved survival outcome [36]. However, this method is difficult to apply to clinical practice.

Recently, entrainment of the brain rhythm with GBO were used as a therapeutic method for AD [26]. Optogenetic stimulation of PV neuron in the hippocampus and visual stimulation at 40 Hz using noninvasive flickering light also decreased Aβ peptides and increased activated microglia in the brain. However, their therapeutic effects were limited to hippocampus and visual cortex, respectively. To achieve a functional improvement, a broader area of the brain needs to be affected by the therapeutic effects. Given the necessity of other stimulation strategy, it is notable that rhythmic auditory stimulations can drive and entrain brain oscillations and this phenomenon is known as 'auditory steady state response (ASSR)' [37]. Depending on the specific frequency stimulus, the auditory beat can induce or inhibit particular frequencies of the brain rhythms [38]. In a clinical pilot study showed that rhythmic sensory stimulation at 40 Hz with sound stimuli improved cognition of AD patients [39]. Therefore, we hypothesized that evoked GBO using 40 Hz acoustic stimulation (AS) can decrease Aβ and increase microglia and the neuropathological improvements may cause neurophysiological benefits, such as normalization of GBO and brain connectivity.

Results

Evoked gamma oscillation facilitates degradation of Aβ plaque with microglia activation.

Aβ plaques were diminished in Tg+/Stim+, but not in Tg+/Stim- (Figure 1a). The number of Aβ plaque decreased in the pre- and infra- limbic(PIL) and hippocampus(HC) regions (46.8% and 60.0% respectively), and it was significantly different between Tg-/Stim- and Tg+/Stim-, Tg-/Stim- and Tg+/Stim+ (Figure 1b, $p<0.01$, $p<0.05$).

Microglia was aggregated in Tg+/Stim+ and Tg+/Stim-, but not in Tg-/Stim- (Figure 1a). There was a significant difference between microglia number per ROI in PIL and HC of Tg+/Stim+, Tg+/Stim- and Tg-/Stim- (Figure 1c, $p<0.01$). Microglia number in PIL and HC increased in Tg+/Stim+ than Tg-/Stim- showed statistical difference (Figure 1c, $p<0.05$, $p<0.01$). And, microglia number increased in PIL and HC (188.3% and 98.9%, respectively), showed no significant difference between Tg+/Stim- and Tg+/Stim- (Figure 1c, $p=0.34$, $p=0.47$). Evoked gamma oscillation facilitates microglia aggregation in Tg+/Stim+ than Tg-/Stim-.

Evoked gamma oscillation decreased Aβ-40, 42 (soluble and insoluble) in PIL

There was a significant difference Aβ level of PIL between Tg+/Stim+, Tg+/Stim- and Tg-/Stim- (Figure 2, $p<0.01$). Tg+/Stim+, Tg+/Stim- have significantly increased Aβ-40, 42 (soluble and insoluble) levels than Tg-/Stim-. ELISA results show significant reduction of soluble Aβ-40 and -42 peptides (45.5% and 67.2%, respectively) in PIL in Tg+/Stim+ compared to Tg+/Stim- (Figure 2, $p<0.05$). On the other hand, there was no statistical difference in other levels of Aβ between Tg+/Stim+ and Tg+/Stim-.

Gamma power in electroencephalography changed after 2 weeks of acoustic stimulation at 40 Hz

We measured the effect of 2 weeks of acoustic stimulation on local field potentials (LFP) to click-trains at gamma band frequency. Wavelet spectral analysis was performed on the averaged waveforms of evoked LFPs within the temporal window of stimulus. Figure 3 show the wavelet power spectral density and scale is corrected for inter-group comparison. Figure 3a show more increased evoked gamma band power on Tg+/Stim+ in day 1 than Tg-/Stim-. Figure 3a also show the reduction of evoked gamma power in Tg+/Stim+ in day 14 than Tg+/Stim-. The data were normalized by its pre-stimulus gamma band power and fold changes were analyzed. Exaggerated evoked gamma power was observed in Tg+/Stim+ in day 1 or Tg+/Stim- (Figure 2b, c). We performed repeated measure analysis of variance (RM ANOVA) for serial follow up with evoked or resting gamma power of Tg+/Stim+ at different time point. Tg+/Stim+ show statistically no significant reduction in evoked gamma power among day 1, 7 and 14 (p = 0.57). Tg+/Stim+ significantly increased resting- spontaneous gamma power (RS-gamma power) in day 7 than day 1, day 14 than day 1 ($p < 0.05$, $p < 0.05$).

Connectivity between frontal and parietal electroencephalography changed after 2 weeks of acoustic stimulation at 40 Hz.

We performed a two-way RM ANOVA for serial follow up with FP connectivity at different groups and time points. FP connectivity was calculated as coherence and phase locking value. Coherence is calculated at evoked gamma duration, and phase locking value(PLV) is calculated at RS gamma period. Figure 4a showed no statistically significant difference in coherence during gamma test of day 1, 7, and 14 (p = 0.108). Tg+/Stim+ showed slight decrement from day 1 to 7, and increment in day 14 (0.82±0.02, 0.73±0.03,

147 0.76±0.03); on the other hand, Tg+/Stim- showed stable value on day 1, 7, and 14 (0.79±0.03,
148 0.79±0.04, 0.78±0.03). Tg-/Stim- showed slight reduction in day 1, 7, or 14 (0.62±0.10,
149 0.56±0.06, 0.57±0.09). Figure 4b showed no statistically significant difference of PLV.
150 Tg+/Stim+ showed increment on day 1, 7, and 14 (0.5±0.1, 0.52±0.11, 0.59±0.07); on the
151 other hand, Tg+/Stim- showed a serial reduction of resting spontaneous gamma phase locking
152 value on day 1, 7, and 14 (0.63±0.03, 0.63±0.06, 0.43±0.15). Tg-/Stim- showed a slight
153 change in phase locking value in day 1, 7, or 14 (0.65±0.05, 0.65±0.1, 0.68±0.08).

154 Phase-amplitude coupling (PAC) changes of the frontal and parietal region in Tg-
155 /Stim-and Tg+/Stim+ in day 1, 14 are observed in Figure 4c, d. PAC patterns including high-
156 gamma activity are analyzed. Top and bottom layer showed that grand-averaged cross-
157 frequency PAC in Tg-/Stim- and Tg+/Stim+ in day 1, 14. PAC is performed as the analysis
158 amplitude (0-160 Hz) and analysis phase (1-16 Hz) combination for F-phase / P-amplitude
159 (top row) and P-phase / F-amplitude (bottom row). The emphasis is that there is low coupling
160 between alpha-phase(F) and high gamma amplitude(P) in Tg+/Stim+ in day 1 (middle
161 column) compared to the Tg-/Stim- (left column) and Tg+/Stim+ in day 14 (right column)
162 (areas highlighted in red square). Delta-phase(P) and evoked gamma-amplitude(F) coupling
163 is exaggerated (areas highlighted in red square) in Tg+/Stim+ in day 1 compared to the Tg-
164 /Stim- and Tg+/Stim+ in day 14. Comparison of maximum PAC values which contain
165 analysis amplitude (30-160 Hz) and alpha phase (8-13 Hz) combination for F-phase / P-
166 amplitude is statistically significant, and comparison of maximum PAC values which contain
167 analysis amplitude (30-160 Hz) and delta phase (1-4 Hz) combination for P-phase / F-
168 amplitude is statistically significant between Tg+/Stim+ in day 1 and day 14 (Figure 4d, $p <$
169 0.05, $p < 0.05$). Mainly coupled frequency of parietal phase with 40Hz frequency of frontal
170 amplitude is high alpha(11-13 Hz) in Tg-/Stim-. That is delta (0-4 Hz) in Tg+/Stim+ in day 1,

171 and is shifted to theta (4-8 Hz).

172

173

Discussion

The AD is characterized by progressive deposition of Aβ and tau protein, resulting in abnormalities of GBO and altered synchronization problems [2,18,40]. Our results showed that 2 weeks of GBO entrainment by acoustic stimulation (AS) at 40Hz facilitated degradation of Aβ plaque with microglia activation. The effects were shown in both PIL cortex and HC which are important areas of the brain for the cognitive function such as executive function and memory. We also found that the evoked GBO were decreased, whereas spontaneous GBO were increased through the stimulation period. Frontal gamma rhythms are coupled with parietal delta at baseline, but the coupling of frontal gamma shifted to parietal theta rhythms after acoustic stimulation.

The number of Aβ plaques in PIL and HC reduced in Tg+/Stim+ than Tg+/Stim- with increased number of microglia. *Post hoc* pairwise comparisons of the number of microglia showed statistical significance only between acoustic stimulation group and wild type, but not between with and without acoustic stimulation. Tg+ mice without acoustic stimulation also showed slight increases of the microglia as a physiological response to increased Aβ, which might reduce the statistical significance. We also performed 2-minute ASSR tests at 40 Hz in day 1, 7 and 14 to measure the evoked GBO responses, which may have caused partial acoustic stimulation effects.

AD has a strong genetic characteristics, and recent observation in genome technology report missense variants in triggering receptor expressed on myeloid cells-2 (TREM2) are correlated with a 2-4 fold increased risk of developing AD [41,42]. TREM2 is essential for Aβ-related microglial responses in mouse models and human. Though the mechanistic basis for reduced microglia is unclear, TREM2 deficiency may cause reduction of microglial response with increased apoptosis, reduced proliferation, or infiltration of peripheral macrophages [43].

198 TREM2 mediates early microglial response, and limits diffusion and toxicity of amyloid
199 plaques [44]. Our results showed that acoustic stimulation at 40 Hz enhanced the microglial
200 response and reduced Aβ deposition. Further researches are warranted to determine whether
201 the effects of acoustic stimulation is mediated by TREM2.

202 We compared our results with previous studies about the recovery of GBO [26,39]. In
203 the study by Iaccarino *et al.* soluble and insoluble Aβ decreased in the target region. Although
204 the optogenetic stimulation and visual flickering methods differ from acoustic stimulation,
205 the common denominator between the two stimuli are the evocation of GBO. In Tg+/Stim+
206 and Tg+/Stim-, the level of soluble and insoluble Aβ was higher than Tg-/Stim-. The level of
207 soluble Aβ-42 was significantly lower in Tg+/Stim+ than Tg+/Stim-, while the level of
208 insoluble Aβ was not statistically significant. The reason why the soluble Aβ decrease
209 significantly, and insoluble Aβ decrease did not show the statistical difference in our results
210 might be the cerebral amyloid angiopathy (CAA) involving capillaries in the progression of
211 the AD [8]. Similarly, when insoluble Aβ was degraded by immunotherapy via activated
212 microglia, CAA might be aggravated. Consequently, inadequate drainage of soluble/insoluble
213 Aβ led to increased micro-hemorrhage and decreased survival outcome [8,29-31].

214 Considering the characteristics of AD mice, in which Aβ deposition is observed from
215 the age of 2 months [45], it is possible that drainage of insoluble Aβ was not performed
216 correctly with progressed CAA due to severe symptoms in 6-month-old mice [46-49] used in this
217 experiment. Although insoluble Aβ might have been degraded to soluble Aβ by microglial
218 activation, insoluble Aβ may remain unaltered in case of progressed CAA [8,29-31]. On the other
219 hand, because 3-month-old mice may not have progressed CAA, the drainage of Aβ would
220 have been intact and thus both soluble and insoluble Aβ decreased in the study of Iaccarino *et*
221 *al*.

These differences suggest that therapeutic methods through degradation of Aβ plaques in patients with progressed dementia should consider the timing of therapeutic point, and the drain pathway of soluble Aβ. Aging is characterized by CSF compartment in brain parenchyma due to cerebral atrophy and decreased cerebrospinal fluid turnover [50]. Choroidal epithelium and ependyma degenerate in aging and also AD. 40% of patients with adult chronic hydrocephalus contain deposition of Aβ [51]. With evidence of decreased CSF Aβ levels have been reported after an internal CSF shunt [52], we suggest a novel combination method of creating CSF shunt for drainage pathway during 40 Hz AS to treat progressed AD patients.

Verrett *et al*. reported the restoration of the GBO after correcting the abnormalities of the VGSC of PV cell followed by the recovery of cognitive function and the reduction of mortality in the AD animal model [36]. In our study, we found that evoked GBO was reduced and the spontaneous GBO was increased, which might be neurophysiological evidence for the functional improvement after acoustic stimulation.

Altered N-methyl-D-aspartate receptors (NMDARs) leads to abnormal function of inhibitory GABAergic interneurons, especially those containing PV interneurons, and the ultimate result is disrupted inhibition of excitatory pyramidal neurons [53,54]. Considering excessive levels of glutamate result in neurotoxicity, NMDAR has been suggested to be a therapeutic target in neurodegenerative disease [54]. Because over-activation of NMDARs cause neurotoxicity, partial NMDAR antagonist (called memantine) blocks the NMDA glutamate receptors to normalize the glutamatergic system and improve cognitive and memory deficits [55]. NMDAR antagonist enhanced resting spontaneous broadband gamma activity [56,57]. We found that spontaneous GBO in Tg+/Stim+ mice which received daily acoustic stimulation for 2 weeks was increased at day 7 and 14. The increase in resting

246 spontaneous GBO is also reported in previous studies to show the therapeutic effectiveness.
247 [18,19,36].

248 We also found the overactivity of GBO evoked by acoustic stimulation in 5XFAD
249 mice. These results are consistent with the previous studies. Measured activities of evoked
250 gamma band power in AD patients was increased compared to the normal group [23,40]. These
251 results are associated with studies that analyzed P50 using a double-click paradigm or
252 auditory steady-state paradigm known as a measure of inhibition of the cortex [21,22]. Several
253 studies using this paradigm in AD patients showed an increase in the amplitude of the second
254 click sound [21]. Similarly, normal controls with a family history of the AD have similar results,
255 suggesting that impaired cortical inhibition may occur very early in the course of AD disease
256 [58]. It is notable that auditory stimulation and response play an essential role in the early
257 diagnosis. A comparative study with patients with mild cognitive impairment (MCI), which is
258 likely to progress AD, as well as patients with the AD, suggests that disorders with abnormal
259 which GBO lead to cognitive impairment were reported [40]. Interestingly, after 14 days of
260 acoustic stimulation, we found a reduction of evoked GBO in Tg+/Stim+ mice than the age-
261 matched Tg+/Stim- mice.

262 Neural synchronization between the frontal and parietal electrodes in 5XFAD mice
263 was analyzed. We only observed trends of increased coherence and decreased phase locking
264 value in 5XFAD, but there was no statistical significance. Theoretically, there is a possibility
265 that the coherence at the gamma frequency increase and the phase locking value decrease in
266 the Tg+/Stim-. For the computation of coherence, both amplitude and frequency of the EEG
267 are utilized. Thus, when the amplitude is large at a certain frequency, the weight becomes
268 larger in the calculation process than other frequencies. Therefore, coherence increases when
269 the acoustic stimulation-evoked gamma band power is increased. On the other hand, in the

case of the instantaneous PLV, it may be effective to observe the functional decrease of the connectivity because only the phase excluding amplitude and frequency is considered. Previous studies have been reported increased coherence in treated AD patients [59,60], and to decrease PLV and global field synchronization in the progression of AD [18-20]. We showed time courses of the decreasing pattern of PLV in Tg+/Stim- mice in comparison with Tg+/Stim+ mice. Two weeks of acoustic stimulation might have contributed to a sustained pattern of PLV, whereas a progressive reduction of PLV was shown for the Tg+/Stim- mice.

Cross frequency phase amplitude coupling (CF-PAC) emphasized that there is lower coupling between alpha-phase(F, frontal) and high gamma amplitude(P, parietal) in Tg+/Stim+ in day 1 compared to wild type mice or Tg+/Stim+ in day 14. During cognitive processing, high gamma CF-PAC is important for effective inter-regional and local communication [9,26]. Alpha-phase high-gamma coupling in wild type mice was suggestive about effective bidirectional modulation from frontal to auditory areas. The reduction of PAC of Tg+ mice in day 1 implies that frontal top-down and parietal bottom-up control may be impaired. This result showed that attention resources could not be appropriately processed. The prefrontal associative cortex is responsible for what is called "top-down" attention, based on the relevance of current tasks to internal goals [40,53,54]. After 2 weeks of acoustic stimulation, PAC between alpha-gamma coupling is increased significantly to the level of wild type mice. Gamma amplitude (F) is coupled with alpha frequency (P) in wild type mice but Tg+ mice showed the strongest coupling between gamma (F) and delta (P). After 2 weeks of acoustic stimulation, the PAC is shifted from gamma (F) – delta (P) to gamma (F) – theta (P). Therefore, acoustic stimulation seemed to cause changes in cross-frequency coupling, which might reflect the improved information processing and cognitive function.

To our best knowledge, this is the first study to confirm the therapeutic effects of

294 acoustic stimulation for GBO entrainment in a mouse model of AD with pathological
295 validation and serial changes of EEG characteristics including GBO, coherence, PLV and
296 CF-PAC. We discovered that 2 weeks of acoustic stimulation at 40 Hz can modify the
297 pathophysiology of Aβ deposition in the cortex of 5XFAD mice, and restoration of GBO and
298 cross-frequency coupling. Further research with acoustic intervention for AD is warranted.
299
300

References

1. Ballard C, Gauthier S, Corbett A, Brayne C, Aarsland D, Jones E. Alzheimer's disease. *The Lancet*.377(9770):1019-1031.
2. Prince MJ. *World Alzheimer Report 2015: the global impact of dementia: an analysis of prevalence, incidence, cost and trends.* Alzheimer's Disease International; 2015.
3. Prince M, Comas-Herrera A, Knapp M, Guerchet M, Karagiannidou M. World Alzheimer report 2016: improving healthcare for people living with dementia: coverage, quality and costs now and in the future. 2016.
4. Houghton P, Howes M-J. Natural products and derivatives affecting neurotransmission relevant to Alzheimer's and Parkinson's disease. *Neurosignals*. 2005;14(1-2):6-22.
5. Hardy J, Selkoe DJ. The amyloid hypothesis of Alzheimer's disease: progress and problems on the road to therapeutics. *Science.* 2002;297(5580):353-356.
6. Cárdenas-Aguayo MdC, Silva-Lucero MdC, Cortes-Ortiz M, et al. Physiological role of amyloid beta in neural cells: the cellular trophic activity. In: *Neurochemistry.* InTech; 2014.
7. Zlokovic BV. Neurovascular pathways to neurodegeneration in Alzheimer's disease and other disorders. *Nature Reviews Neuroscience*. 2011;12(12):723-738.
8. Weller R, Subash M, Preston S, Mazanti I, Carare R. Perivascular drainage of amyloid-b peptides from the brain and its failure in cerebral amyloid angiopathy and Alzheimer's disease. *Brain Pathol*. 2008;18(2):253-266.
9. Carare R, Bernardes-Silva M, Newman T, et al. Solutes, but not cells, drain from the brain parenchyma along basement membranes of capillaries and arteries: significance

for cerebral amyloid angiopathy and neuroimmunology. *Neuropathol Appl Neurobiol.* 2008;34(2):131-144.

10. Szentistvanyi I, Patlak CS, Ellis RA, Cserr HF. Drainage of interstitial fluid from different regions of rat brain. *American Journal of Physiology-Renal Physiology.* 1984;246(6):F835-F844.

11. Cserr HF, Harling-Berg CJ, Knopf PM. Drainage of brain extracellular fluid into blood and deep cervical lymph and its immunological significance. *Brain Pathol.* 1992;2(4):269-276.

12. Abbott A, Dolgin E. Failed Alzheimer's trial does not kill leading theory of disease. *Nature.* 2016;540(7631):15-16.

13. Salinas E, Sejnowski TJ. Correlated neuronal activity and the flow of neural information. *Nature reviews neuroscience.* 2001;2(8):539-550.

14. Herrmann CS, Munk MH, Engel AK. Cognitive functions of gamma-band activity: memory match and utilization. *Trends Cogn Sci.* 2004;8(8):347-355.

15. Başar E, Başar-Eroglu C, Karakaş S, Schürmann M. Gamma, alpha, delta, and theta oscillations govern cognitive processes. *Int J Psychophysiol.* 2001;39(2):241-248.

16. Kaiser J, Lutzenberger W. Induced gamma-band activity and human brain function. *The Neuroscientist.* 2003;9(6):475-484.

17. Buzsaki G, Wang XJ. Mechanisms of gamma oscillations. *Annu Rev Neurosci.* 2012;35:203-225.

18. König T, Prichep L, Dierks T, et al. Decreased EEG synchronization in Alzheimer's disease and mild cognitive impairment. *Neurobiology of aging.* 2005;26(2):165-171.

19. Stam C, Van Der Made Y, Pijnenburg Y, Scheltens P. EEG synchronization in mild cognitive impairment and Alzheimer's disease. *Acta Neurol Scand.* 2003;108(2):90-96.

20. Herrmann C, Demiralp T. Human EEG gamma oscillations in neuropsychiatric disorders. *Clin Neurophysiol.* 2005;116(12):2719-2733.

21. Cancelli I, Cadore IP, Merlino G, et al. Sensory gating deficit assessed by P50/Pb middle latency event related potential in Alzheimer's disease. *Journal of clinical neurophysiology.* 2006;23(5):421-425.

22. Potter D, Summerfelt A, Gold J, Buchanan RW. Review of clinical correlates of P50 sensory gating abnormalities in patients with schizophrenia. *Schizophr Bull.* 2006;32(4):692-700.

23. Osipova D, Pekkonen E, Ahveninen J. Enhanced magnetic auditory steady-state response in early Alzheimer's disease. *Clin Neurophysiol.* 2006;117(9):1990-1995.

24. Hsieh H, Boehm J, Sato C, et al. AMPAR removal underlies Aβ-induced synaptic depression and dendritic spine loss. *Neuron.* 2006;52(5):831-843.

25. Kamenetz F, Tomita T, Hsieh H, et al. APP processing and synaptic function. *Neuron.* 2003;37(6):925-937.

26. Iaccarino HF, Singer AC, Martorell AJ, et al. Gamma frequency entrainment attenuates amyloid load and modifies microglia. *Nature.* 2016;540(7632):230-235.

27. Wilcock DM, DiCarlo G, Henderson D, et al. Intracranially administered anti-Aβ antibodies reduce β-amyloid deposition by mechanisms both independent of and associated with microglial activation. *J Neurosci.* 2003;23(9):3745-3751.

28. Wilcock DM, Rojiani A, Rosenthal A, et al. Passive amyloid immunotherapy clears amyloid and transiently activates microglia in a transgenic mouse model of amyloid deposition. *J Neurosci.* 2004;24(27):6144-6151.

29. Nicoll JA, Wilkinson D, Holmes C, Steart P, Markham H, Weller RO. Neuropathology of human Alzheimer disease after immunization with amyloid-β

peptide: a case report. *Nat Med.* 2003;9(4):448-452.

30. Boche D, Zotova E, Weller R, et al. Consequence of Aβ immunization on the vasculature of human Alzheimer's disease brain. *Brain.* 2008;131(12):3299-3310.

31. Wilcock DM, Rojiani A, Rosenthal A, et al. Passive immunotherapy against Aβ in aged APP-transgenic mice reverses cognitive deficits and depletes parenchymal amyloid deposits in spite of increased vascular amyloid and microhemorrhage. *J Neuroinflammation.* 2004;1(1):24.

32. Schenk D, Barbour R, Dunn W, et al. Immunization with amyloid-β attenuates Alzheimer-disease-like pathology in the PDAPP mouse. *Nature.* 1999;400(6740):173-177.

33. Patton RL, Kalback WM, Esh CL, et al. Amyloid-β peptide remnants in AN-1792-immunized Alzheimer's disease patients: a biochemical analysis. *The American journal of pathology.* 2006;169(3):1048-1063.

34. Holmes C, Boche D, Wilkinson D, et al. Long-term effects of Aβ 42 immunisation in Alzheimer's disease: follow-up of a randomised, placebo-controlled phase I trial. *The Lancet.* 2008;372(9634):216-223.

35. Lewis DA, Hashimoto T, Volk DW. Cortical inhibitory neurons and schizophrenia. *Nature Reviews Neuroscience.* 2005;6(4):312-324.

36. Verret L, Mann EO, Hang GB, et al. Inhibitory interneuron deficit links altered network activity and cognitive dysfunction in Alzheimer model. *Cell.* 2012;149(3):708-721.

37. Thut G, Schyns P, Gross J. Entrainment of perceptually relevant brain oscillations by non-invasive rhythmic stimulation of the human brain. *Front Psychol.* 2011;2:170.

38. Becher AK, Höhne M, Axmacher N, Chaieb L, Elger CE, Fell J. Intracranial

electroencephalography power and phase synchronization changes during monaural and binaural beat stimulation. *Eur J Neurosci.* 2015;41(2):254-263.

39. Clements-Cortes A, Ahonen H, Evans M, Freedman M, Bartel L. Short-term effects of rhythmic sensory stimulation in Alzheimer's disease: An exploratory pilot study. *J Alzheimers Dis.* 2016;52(2):651-660.

40. Van Deursen J, Vuurman E, van Kranen-Mastenbroek V, Verhey F, Riedel W. 40-Hz steady state response in Alzheimer's disease and mild cognitive impairment. *Neurobiol Aging.* 2011;32(1):24-30.

41. Jonsson T, Stefansson H, Steinberg S, et al. Variant of TREM2 associated with the risk of Alzheimer's disease. *N Engl J Med.* 2013;368(2):107-116.

42. Guerreiro R, Wojtas A, Bras J, et al. TREM2 variants in Alzheimer's disease. *N Engl J Med.* 2013;368(2):117-127.

43. Ulrich JD, Holtzman DM. TREM2 function in Alzheimer's disease and neurodegeneration. *ACS Chem Neurosci.* 2016;7(4):420-427.

44. Wang Y, Ulland TK, Ulrich JD, et al. TREM2-mediated early microglial response limits diffusion and toxicity of amyloid plaques. *J Exp Med.* 2016:jem. 20151948.

45. Oakley H, Cole SL, Logan S, et al. Intraneuronal β-amyloid aggregates, neurodegeneration, and neuron loss in transgenic mice with five familial Alzheimer's disease mutations: potential factors in amyloid plaque formation. *J Neurosci.* 2006;26(40):10129-10140.

46. Ohno M. Failures to reconsolidate memory in a mouse model of Alzheimer's disease. *Neurobiol Learn Mem.* 2009;92(3):455-459.

47. Lison H, Happel M, Schneider F, et al. Disrupted cross-laminar cortical processing in β amyloid pathology precedes cell death. *Neurobiol Dis*. 2014;63:62-73.

421 48. Kimura R, Ohno M. Impairments in remote memory stabilization precede
422 hippocampal synaptic and cognitive failures in 5XFAD Alzheimer mouse model.
423 *Neurobiol Dis.* 2009;33(2):229-235.
424 49. Schneider F, Baldauf K, Wetzel W, Reymann K. Behavioral and EEG changes in male
425 5xFAD mice. *Physiology & behavior.* 2014;135:25-33.
426 50. Sakka L, Coll G, Chazal J. Anatomy and physiology of cerebrospinal fluid. *Eur Ann*
427 *Otorhinolaryngol Head Neck Dis.* 2011;128(6):309-316.
428 51. Golomb J, Wisoff J, Miller D, et al. Alzheimer's disease comorbidity in normal
429 pressure hydrocephalus: prevalence and shunt response. *J Neurol Neurosurg*
430 *Psychiatry.* 2000;68(6):778-781.
431 52. Silverberg GD, Mayo M, Saul T, Rubenstein E, McGuire D. Alzheimer's disease,
432 normal□pressure hydrocephalus, and senescent changes in CSF circulatory
433 physiology: a hypothesis. *The Lancet Neurology.* 2003;2(8):506-511.
434 53. Carlen M, Meletis K, Siegle J, et al. A critical role for NMDA receptors in
435 parvalbumin interneurons for gamma rhythm induction and behavior. *Mol Psychiatry.*
436 2012;17(5):537-548.
437 54. Paoletti P, Bellone C, Zhou Q. NMDA receptor subunit diversity: impact on receptor
438 properties, synaptic plasticity and disease. *Nature Reviews Neuroscience.*
439 2013;14(6):383-400.
440 55. Olivares D, K Deshpande V, Shi Y, et al. N-methyl D-aspartate (NMDA) receptor
441 antagonists and memantine treatment for Alzheimer’s disease, vascular dementia and
442 Parkinson’s disease. *Current Alzheimer Research.* 2012;9(6):746-758.
443 56. Lazarewicz MT, Ehrlichman RS, Maxwell CR, Gandal MJ, Finkel LH, Siegel SJ.
444 Ketamine modulates theta and gamma oscillations. *J Cogn Neurosci.*

2010;22(7):1452-1464.

57. Pinault D. N-methyl d-aspartate receptor antagonists ketamine and MK-801 induce wake-related aberrant γ oscillations in the rat neocortex. *Biol Psychiatry.* 2008;63(8):730-735.

58. Boutros N, Torello MW, Burns EM, Wu S-S, Nasrallah HA. Evoked potentials in subjects at risk for Alzheimer's disease. *Psychiatry Res.* 1995;57(1):57-63.

59. Başar E, Schmiedt-Fehr C, Mathes B, et al. What does the broken brain say to the neuroscientist? Oscillations and connectivity in schizophrenia, Alzheimer's disease, and bipolar disorder. *Int J Psychophysiol.* 2016;103:135-148.

60. Başar E, Femir B, Emek-Savaş DD, Güntekin B, Yener GG. Increased long distance event-related gamma band connectivity in Alzheimer's disease. *NeuroImage: Clinical.* 2017;14:580-590.

61. Osipova D, Hermes D, Jensen O. Gamma power is phase-locked to posterior alpha activity. *PLoS One.* 2008;3(12):e3990.

62. Canolty RT, Edwards E, Dalal SS, et al. High gamma power is phase-locked to theta oscillations in human neocortex. *Science.* 2006;313(5793):1626-1628.

Materials and methods

2.1 Animals

Adult (5-month-old) male 5XFAD mice were prepared. The 5XFAD mouse model (Tg6799, Stock 6554) was purchased from Jackson Laboratory. This model is a double transgenic that overexpresses not only PS1 M146L and L286V but also APP Swedish, Florida and London mutations, which are under the control of the murine Thy-1-promoter. Swedish mutation produces higher levels of total Aβ; on the other hand, Florida, London, M146L, and L286V mutations characteristically increase the production of $A\beta_{x\text{-}42}$. Mice of the B6SJLF1 / J background strain have high APP expression correlated with accelerated accumulation of $A\beta_{x\text{-}42}$ in comparison to $A\beta_{x\text{-}40}$. 21 males were used in this experiment, and all mice were handled with Gwangju Institute Science and Technology (GIST) Laboratory Animal Resource Center (LARC) guidelines for animal care. Mice were bred and kept in a 12/12 hour light-dark cycle (light on at 9 a.m.) a temperature and humidity controlled room at 20°C ± 2°C, 55%±5%. Water and food were freely available *ad libitum*. All animal procedures have been approved by the ethics committee of GIST LARC which fulfilled with Association for Assessment and Accreditation of Laboratory Animal Care International guidelines. 15 males were 5XFAD mice, and 6 males were their wild-type littermates. 3 of 15 5XFAD males underwent behavioral tests before sound stimulation and after 2 weeks of sound stimulation. 12 of 15 5XFAD males were randomly separated into 2 groups. Group 1 [Tg(+)(ASSR(+)) consisted of 7 mice stimulated for 2 hours per day for 2 weeks. Group 2 [Tg(+)ASSR(-)] consisted of 5 mice and group 3 [wild-type littermates] consisted of 6 mice that simply received gamma test at day 0, 7, and 14.

2.2 Surgical preparation, electrode implantation

The animal was anesthetized with 4% isoflurane and maintained with 0.5 to 1.5% isoflurane in a stereotaxic frame. 0.1mg/kg of ketofen was injected subcutaneously before surgery to control pain. The blanket was used to maintain body temperature. Mouse eye was covered with protecting ointment. After shaving incision line, incision of the midline using scalpel and the cranium was exposed, five holes of 0.8mm were drilled over the frontal (AP: 1.0 mm, ML: 1.0 mm), parietal (AP: -3.5 mm, ML: 1.0 mm), ground (AP: -2.0 mm, ML: 1.5 mm), anchor (AP: -2.0 mm, ML: -1.5 mm), and reference (AP: -5.3 mm, ML: 0.0 mm). EEG electrodes of screw type were inserted at a depth that would hardly touch or touch the brain in drilled holes, and EMG electrodes were inserted in neck muscles. 1x2mm screws were inserted as an anchor for a metal holder that was cemented to the skull with dental cement. The screws with wire were fixed with dental cement, and after the cement had completely hardened, the remnant parts of wires and the connector (PINNACLE Technology Inc, Oregon, US) were fixed on the vertex of the skull by soldering and dental cement. In the end, the simple suture was performed after wound irrigation. Animals were then housed in a cage for more than 1 week for postoperative recovery.

2.3 In Vivo EEG/EMG Recordings

Continuous EEG/EMG (8200-K1-SL amplifier; Pinnacle Technology) were recorded before, during, and after 40 Hz auditory stimulation. We were careful about circadian timing and performed 2-hour auditory stimulation and recorded EEG from 22:00 (ZT 13) to 00:00 (ZT 15). This ensured that the animals were in their physiologic activity, and reduced the period of falling asleep during a stimulation session. Sleep was monitored with EEG/EMG signals. The EEG/EMG signal (2 KHz sampling, 100 Hz lowpass filtered; Pinnacle PAL8200/Sirenia software) response to auditory stimulation was recorded using WinWCP software

(Strathclyde Institute of Pharmacy and Biomedical Sciences).

2.4 Auditory stimulus

Auditory clicks (20 rectangular pulses of 10ms duration per 500ms, 40Hz) per sec were generated by custom-built programs under WinWCP (Strathclyde Institute of Pharmacy and Biomedical Sciences) condition and delivered via a speaker, which created the sound pressure of 90dB in the soundproof room. There was a stimulation time of 500ms and a resting time of 700ms with a cycle of 1.2 seconds. The resting time consisted of the system time for the next recording of 200ms and the recording time, which is consisted of 250ms before stimulation and 250ms after stimulation. Recording and click trains were 1 cycle/sec, and each train had 200ms interval. In the end, the mice received 6000 cycles of the train for 2 hours every day. We performed gamma tests at 0, 7, 14 days of an experiment to check the gamma response between the groups. The gamma test is repeated 200 cycles of the above 1.2 seconds cycle, which takes a total of 4 minutes.

2.5 EEG Data Analysis

Offline processing was performed in the customized code for Matlab. Wavelet transformation (WT; continuous wavelet from Matlab Wavelet Toolbox; frequencies represented from 1 to 100 Hz) was performed. WT power was measured from 38 to 42 Hz gamma band.

We calculated magnitude-squared coherence between frontal and parietal epidural electrode. Using mscohere function in MatLab, we obtained sequences frontal and parietal EEG before and after stimulation for inspecting connectivity changes between frontal and parietal region.

We also calculated phase locking value (PLV). For calculation of PLVs, the length of the time window that is required to obtain instantaneous phase information should be determined. We

defined this window at resting spontaneous (pre-stimulation) period into 230ms lengths and stimulation period into 460ms lengths. Before the Hilbert transform, the frequency of interest should be determined. Local field potentials were filtered using a second order bandpass digital Butterworth filter with a higher and lower cut off adjusted to 2 Hz above and below the stimulus frequency. For example, lower and upper corner frequencies of 38 and 42 Hz respectively were used for the 40-Hz stimulus. PLV is defined as an average of the differences of instantaneous phase between the two signals. The PLVs have a range of values from 0 to 1, that indicates no phase locking to complete phase locking. Averaged evoked power, frontal-parietal coherence, phase-locking data were quantified. Gamma band wavelet power expressed evoked data relative to the resting spontaneous(pre-stimulus) data or resting spontaneous data itself.

Cross-frequency coupling (CFC) between frontal and parietal electrode was evaluated using the PAC values. We calculated the coherence between a low-frequency signal and the time-course of the power at the higher frequency. Signals containing phase was at 1 to 16 Hz, and signals containing amplitude was at 30 to 160 Hz. PAC values were calculated for each frequency pair for LFP recorded during auditory stimulation. The PAC analysis was conducted on the 60 Hz notch- filtered EEG data. To generate color-maps shown in the figure, we use grand averaged EEG in a particular group (Tg-/Stim-, Tg+/Stim- and Tg+/Stim+). To calculate spectrograms of EEG activity averaged at low-frequency phase troughs with the highest PAC, signals were first filtered in the delta band using a narrow band-pass filter (a symmetrical finite impulse response filter with a specific nesting frequency within the delta frequency range [1-4 Hz]), and then amplitude troughs were identified from the filtered signals. Using Brainstorm software, a time-frequency decomposition was performed to obtain the power of all averaged time-frequency plots. Alpha (8-13 Hz) phase and gamma (40-160

Hz) amplitude cross-frequency coupling were investigated based on papers that the phase of lower frequency oscillations modulate the amplitude of gamma oscillations [61,62]. The maximum PAC values of these frequency ranges were analyzed among Tg-/Stim-, Tg+/Stim+ in day 1 and 14.

2.6 Immunoassay and immunohistochemistry

Mouse brain homogenization

Mice were deeply anesthetized by intraperitoneal injection of Zoletil (Virbac, SA, Carros, France), and then transcardiacally perfused with filtered PBS. Brains were removed, dissected, frozen in dry-ice cold isopentane (Sigma-Aldrich, St. Louis, MO, USA), and stored at -80 °C until use. Medial prefrontal cortex (mPFC) was extracted as 1:4 (4 μl/mg of brain) of ice-cold TBS extraction buffer (50 mM Tris-buffered saline, pH 7.6) containing complete protease inhibitor cocktail (Roche Diagnostics) using a tissue grinder with Teflon pestle on ice. The homogenates were centrifuged at a speed of 200,000 g for 20 min at 4°C (Beckman Optima TL Ultracentrifuge, TLA100.4 rotor). The supernatants (TBS-soluble fraction) were kept at -80 °C before the assay. After adding 4 volumes (based on initial hemisphere weight) of 6M GuHCl solution (6M GuHCl, 50 mM Tris-HCl, protease inhibitor cocktail, pH 7.6), samples were incubated in 6M GuHCl solution for 1 hr at 25°C and finally centrifuged at a speed 200,000 g for 20 min at 4°C to extract GuHCl-soluble fraction.

Sandwich Enzyme linked immunesorbent assay (ELISA)

Levels of amyloid beta 1-40 and 1-42 in the brain extracts were assayed with sandwich ELISA kit (#KHB3481 for amyloid beta 1-40, #KHB3441 for amyloid beta 1-42, Thermo Scientific) according to the manufacturer's guidance. Optical densities (at 450 nm) were

588 measured by Tecan Infinite F50 microplate reader (TECAN, Austria). Assay sensitivity was
589 <6 pg/ml for amyloid beta 1-40 and <10 pg/ml for amyloid beta 1-42.
590
591 **Immunohistochemistry**
592 Brains were fixed in 4% paraformaldehyde solution for overnight, and then placed in 30%
593 sucrose solution at 4 °C until they sink. Serial coronal sections (30-µm thickness) of the
594 whole brain were obtained and were stored in cryoprotectant solution (30% RNase free
595 sucrose, 30% ethylene glycol, and 1% polyvinyl pyrrolidine in 100 mM, pH 7.4) at -20 °C.
596 All immunohistochemical stainings were executed using the free-floating method as
597 described below. Samples were incubated in 70% formic acid solution for 10 min, washed,
598 and then incubated in 1% H 2 O 2 in 0.1 M PBS (pH 7.4) for 10 min to block endogenous
599 peroxidase activity. Tissues were reacted in a buffer containing 0.2% Triton X-100 (PBS-T),
600 10% normal goat serum (NGS) for 1 h. Sections were then incubated for 3 days at 4°C with a
601 mouse anti-amyloid beta 1-42 (1:1,000; Biolegend) or rabbit anti-iba-1 antibody (1:1000;
602 Wako Pure Chemical Industries, Osaka, Japan, #019-19741). After washing, they were
603 incubated with biotinylated goat anti-mouse IgG (1:1,000; Vector Laboratories, Burlingame,
604 CA, USA) or biotinylated goat anti-rabbit IgG (1:1,000; Vector Laboratories) for 12–24 h at
605 4 °C. After several rinses with PBS-T, the sections were incubated in an avidin–biotin–
606 peroxidase complex (1:250; Vector Laboratories) for 1 h. After rinsing, sections were
607 incubated for 10 min in 0.05% (w/v) diaminobenzidine solution containing 0.3% H 2 O 2 .
608 The sections were then washed
609 with PBS, mounted on glass slides, dried overnight, dehydrated, and cover-slipped under
610 Permount (Fisher Scientific, Fair Lawn, NJ, USA). Images showing immunoreactivites were
611 captured using a ProGress C14 camera (Jenoptik,Jena, Germany) mounted on a Zeiss

axioscope microscope (Zeiss, Germany).

2.7 Statistics

Normal distribution of data was validated with Kolmogorov-Smirnov test and Shapiro-Wilk test. For group comparison at a separate time point, we used the one-way ANOVA followed by the Bonferroni multiple comparisons for normally distributed data and Kruskal-Walis and Mann-Whitney Rank Sum Test for non-normally distributed data. Serial data was analyzed with repeated measure analysis of variance (RM ANOVA). The interaction between variables was also calculated. All data are shown as an average ± standard error of the means (S.E.M). The statistical significance levels are indicated by one or two asterisks in figures (*$p<0.05$, **$p<0.01$).

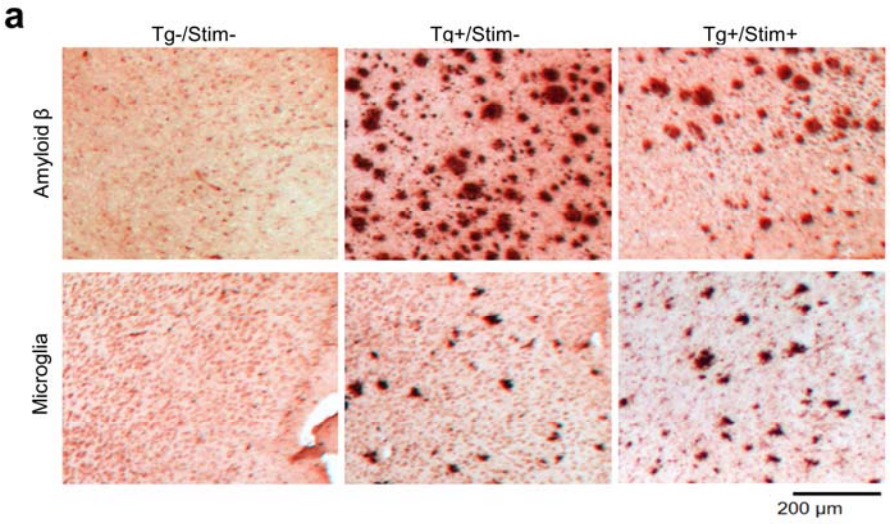

634

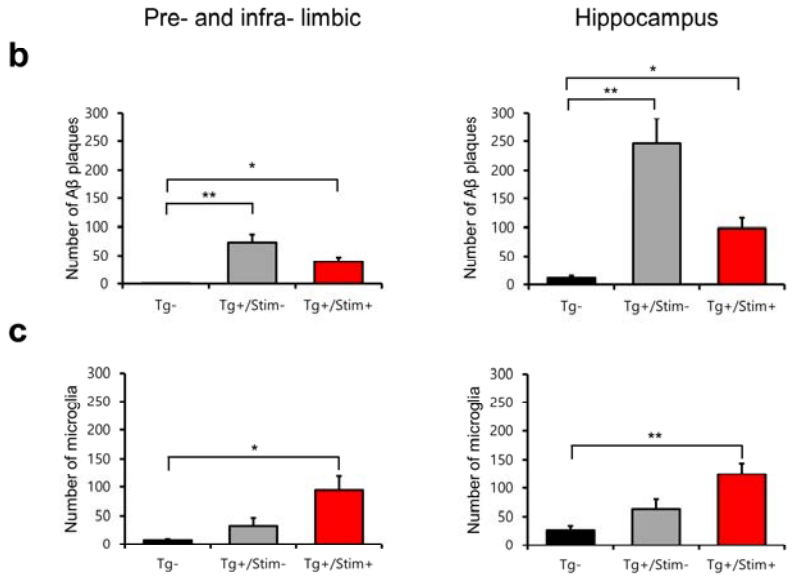

635

636 **Fig. 1 Reduced number of amyloid beta (Aβ) plaques in 5XFAD mice after acoustic stimulation at 40**
637 **Hz. a** Representative histologic findings with the immunohistochemistry for Aβ (*upper row*) and
638 microglia (*bottom row)* in the pre- and infra-limbic cortex. **b, c** Quantification of the number of Aβ
639 plaques and microglia in the pre- and infra-limbic cortex and hippocampus, respectively. Black, red,
640 and gray bars indicate Tg-, Tg+/Stim+, and Tg+/Stim-, respectively. $^{*}p < 0.05$, $^{**}p < 0.01$ Mann-
641 Whitney test following Kruskal-Wallis test or Dunnett T3, Bonferroni(equal variance assumed) *post-*
642 *hoc* test following ANOVA test.

643

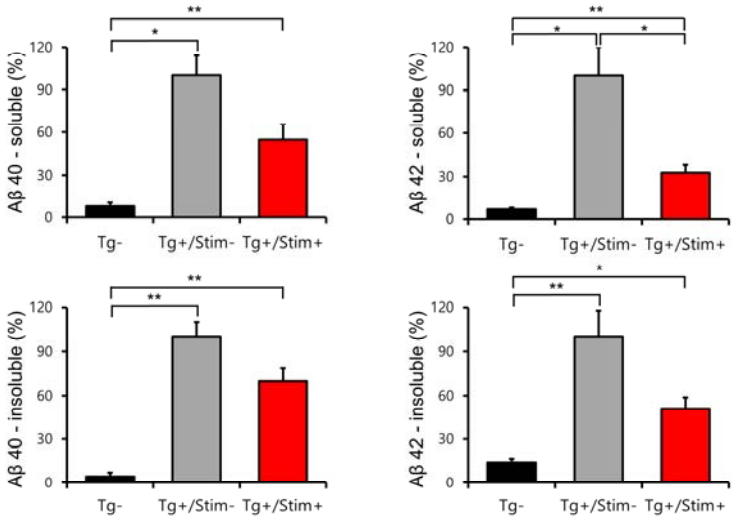

Fig. 2 Reduced soluble Aβ40 and Aβ42 levels in pre- and infra-limbic after acoustic stimulation at 40 Hz. Black, red, and gray bars indicate Tg-, Tg+/Stim+, and Tg+/Stim-, respectively. $^{*}p < 0.05$, $^{**}p < 0.01$ Mann-Whitney test following Kruskal-Wallis test or *post-hoc* Dunnett T3 test following ANOVA test with welch correction.

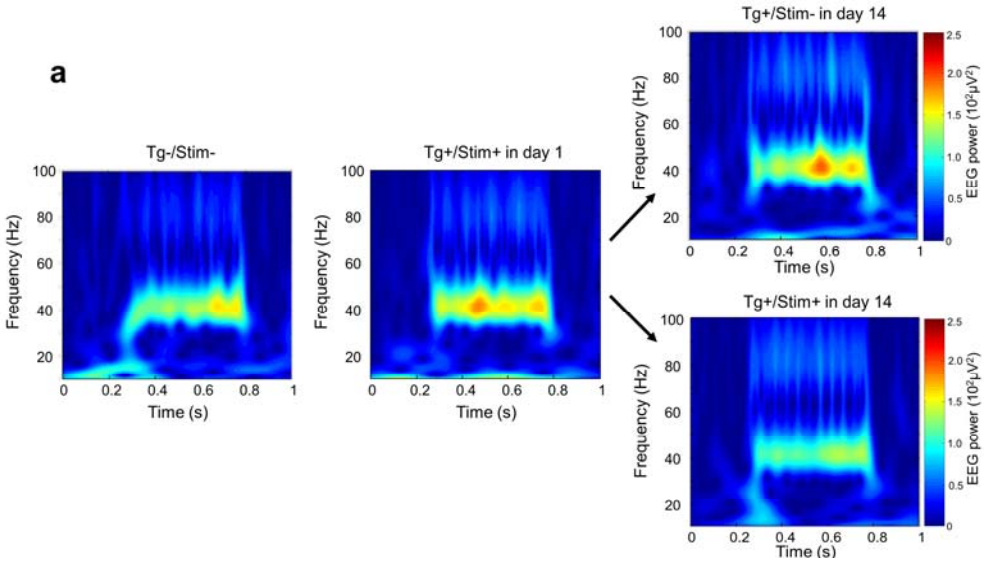

634

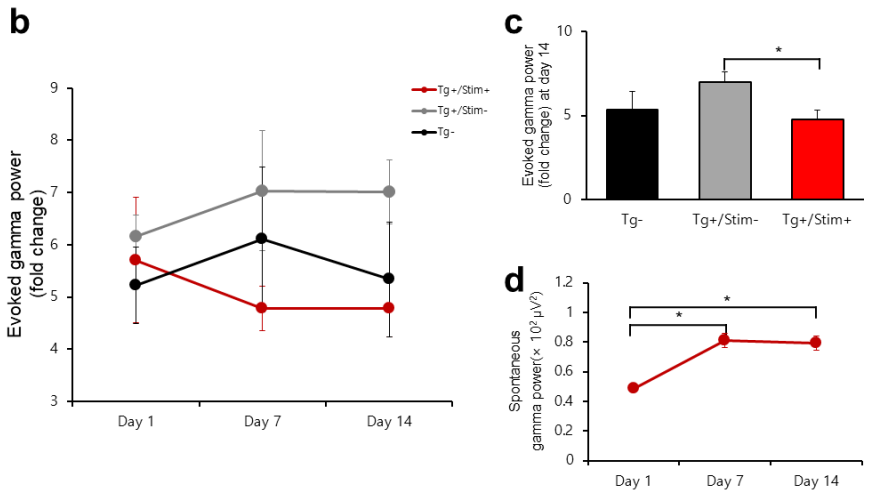

635

636 **Fig. 3 Evoked and spontaneous gamma power in electroencephalography changed after 2 weeks of**
637 **acoustic stimulation at 40 Hz. a** Time-frequency analysis of the grand averaged EEG data from the
638 auditory steady-state response (ASSR) at 40Hz using the wavelet transformation. **b** Time course of
639 the evoked gamma power in Tg-, Tg+/Stim-, and Tg+/Stim+ groups at the stimulation day 1, 7, and 14.
640 Tg+/Stim+ was not statistically significant by repeated measure ANOVA. **c** The evoked gamma power
641 at day 14 in Tg-, Tg+/Stim-, and Tg+/Stim+ groups, depicted as black, gray and red bars, respectively.
642 There is statistical difference between Tg+/Stim- and Tg+/Stim+. *P<0.05 by Mann-Whitney test. **d**
643 Time course of resting gamma power in Tg+/Stim+ group. *P<0.05 by Bonferroni correction following
644 repeated measure ANOVA.

634

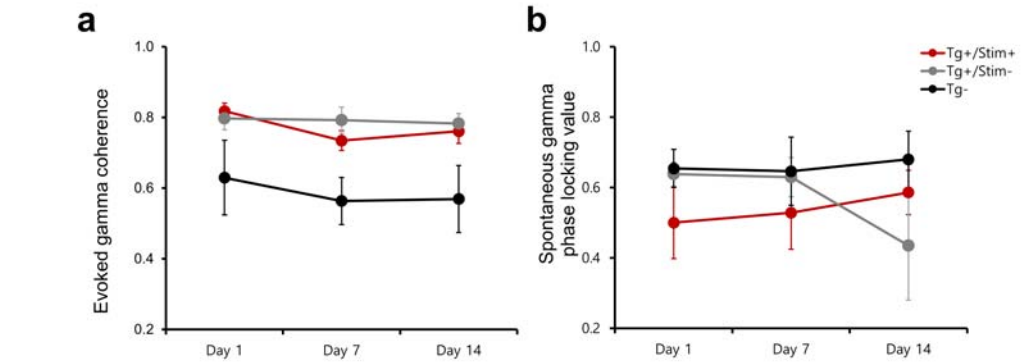

635

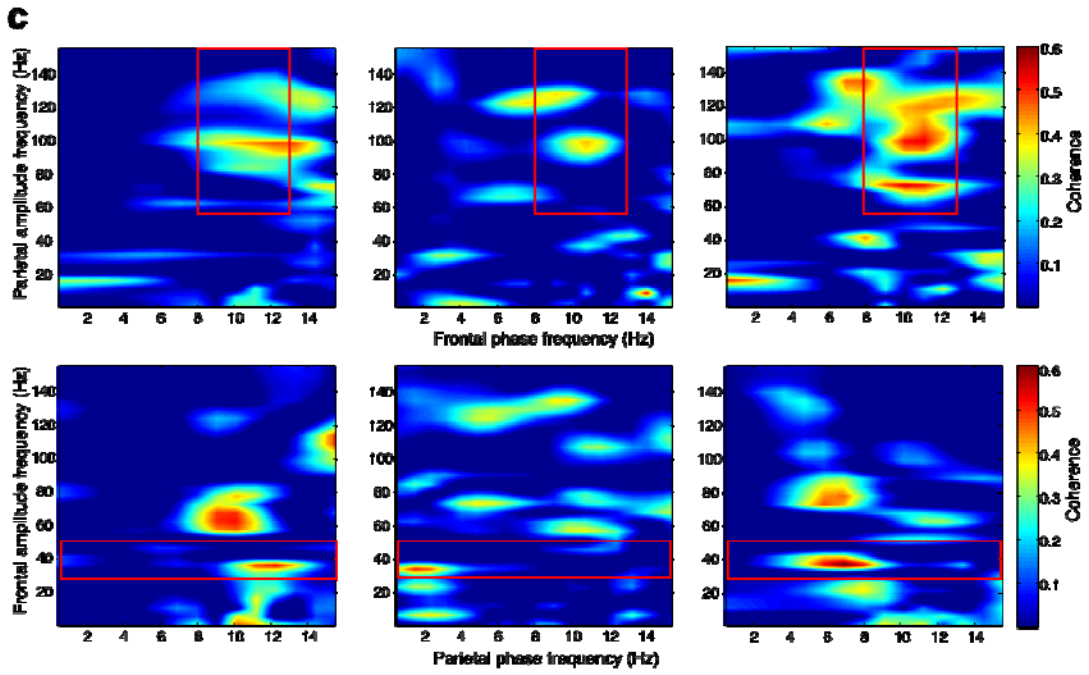

636

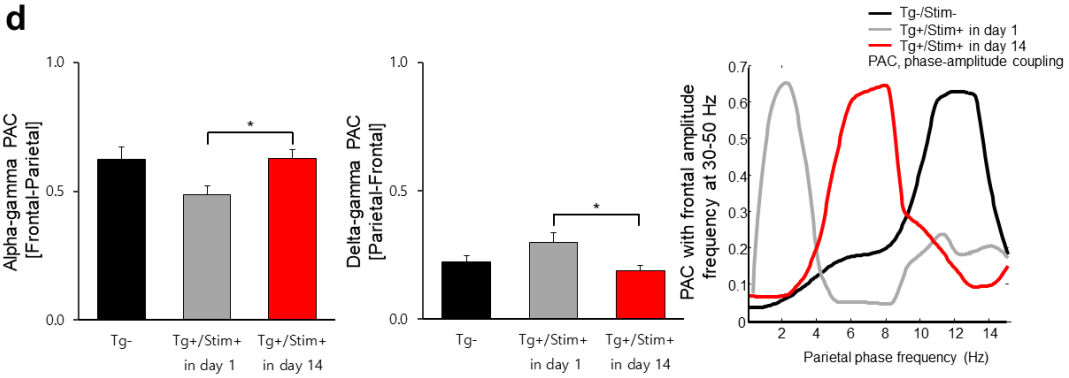

637

634 **Fig. 4 Connectivity between frontal and parietal electroencephalography changed after 2 weeks of**
635 **acoustic stimulation at 40 Hz.**

636 **a, b** Time course of the evoked gamma coherence and the resting gamma phase locking value. Tg-,
637 Tg+/Stim-, and Tg+/Stim+ groups were depicted as black, gray and red circles and lines, respectively.
638 Tg+/Stim+ was not statistically significant by repeated measure ANOVA. **c** Cross-frequency phase-
639 amplitude coupling (PAC) of the frontal and parietal grand-averaged EEG during the auditory steady-
640 state response tests. Parietal amplitude frequency and frontal phase frequency coupling (*upper row*)
641 and frontal amplitude frequency and parietal phase frequency coupling (*bottom row*) were plotted. The
642 color bar indicates coherence (ranging from 0 to 1), with no coherence (0) to perfect coherence (1).
643 Red rectangles represent the area of interest (ROI). **d** Quantification of the maximal PAC values in the
644 ROIs. Black, gray and red bars represent Tg-, Tg+/Stim+ at baseline, and Tg+/Stim+ at day 14,
645 respectively. *P<0.05 by *post-hoc* Bonferroni test following ANOVA.

646